EVOLUTIONARY BIOLOGY

The 3D architecture of the ctenophore aboral organ and the evolution of complex integrative centers in animals

Anna Ferraioli[1], Leonid Digel[1], Daniela Sturm[1], Jeffrey Colgren[1], Carine Le Goff[1], Alexandre Jan[1], Joan J. Soto-Angel[1], Benjamin Naumann[2], Maike Kittelmann[3]*, Pawel Burkhardt[1]*

The ability to sense and respond to environmental cues is fundamental to animal behavior and survival. In ctenophores—early-branching marine animals—a subepitheliall nerve net (SNN) underlies complex behaviors such as geotaxis, feeding, and escape. Central to this system is the aboral organ (AO), a sensory hub that detects motion, light, and pressure and coordinates ciliary movement. However, the AO's cellular architecture and its integration with the SNN remain poorly understood. Here, using volume electron microscopy in *Mnemiopsis leidyi*, we reveal that the SNN condenses around the AO, forming synaptic connections with effector cells. We annotated 17 cell types, including nonsynaptic vesicle-rich cells likely involved in volume transmission. Our data suggest that signal processing within the AO relies on synaptic and nonsynaptic communication. Profiling of shared cnidarian-bilaterian transcription factors revealed nonconserved expression, suggesting unique molecular pathways underlying ctenophore AO formation. Our findings redefine the ctenophore AO as a distinct, integrated, and potentially multimodal sensory system critical for behavioral regulation.

INTRODUCTION

Approximately 560 million years ago, the earliest animals (metazoans) having distinct nervous systems began to diversify (*1*, *2*). These early nervous systems were likely organized as diffuse nerve nets that directly innervated contractile cells, enabling coordinated body contractions for locomotion and feeding while also integrating inputs from sensory cells and receptors (*3*, *4*). These sensory components allowed early animals to explore their surroundings and react to dynamic environmental conditions. Whether the capacity to integrate external and/or internal inputs has evolved only once or whether convergent evolutionary pathways led to the present diversity of sensory systems in animals remains unresolved. To address these questions, further analysis of sensory systems across early diverging animal phyla is required.

The placement of sponges (Porifera), which lack neurons and a nervous system, as the earliest-branching animals (*5*–*9*) is challenged by the placement of comb jellies (Ctenophora), which have neurons and a nervous system, as the sister group to all other living metazoan lineages (Fig. 1A) (*10*–*13*). This sparked discussions on the independent evolution of organ systems and cell types. One of the most controversial topics is the potential independent origin of neurons, nervous systems, and their organization, along with specialized sensory cells, which combine within the elaborate integrative systems of animals (Fig. 1A) (*11*).

Most extant ctenophores are pelagic, direct-developing marine invertebrates characterized by a biradial symmetry, tentacles with adhesive colloblasts for prey capture, and a unique swimming mode driven by beating macrocilia organized into eight comb rows (*14*–*17*). These comb rows connect to the subepithelial nerve net (SNN) and, via ciliated grooves, to the aboral organ (AO) (*17*–*19*). The AO develops after gastrulation is completed and persists throughout life in all pelagic species (*19*). It modulates important behaviors such as feeding, vertical migration, and escape responses based on photo, pressure, and gravity sensation (*16*, *20*–*22*). The AO consists of an epithelial floor composed of densely packed ciliated cells, a statolith suspended by four balancer cilia, and putative secretory, photo-, and pressure-sensitive cells. The entire structure is shielded from the environment by a ring of long ciliated cells forming a dome-like cover (Fig. 1, B and C). Aboral or apical sensory organs are found in other metazoan lineages and are specific to larval stages (*23*). The apical organ of cnidarian planula larvae comprises a diverse assemblage of different sensory neurons, gland cells, and, in some anthozoan larvae, long-ciliated epithelial cells forming an apical tuft (*24*–*26*). It is associated with a larval nerve plexus and initiates larval tissue degeneration at the onset of metamorphosis into a benthic polyp (*27*, *28*). In *Nematostella vectensis* planula, the apical organ consists of sensory and support cells (*26*). The apical organ of many bilaterian larvae consists of a conserved set of ciliated sensory neurons, support cells, photosensitive cells, and neurosecretory cells (*24*, *26*, *29*, *30*). As in cnidarians, it is often associated with a neural plexus (*24*) and is involved in metamorphosis in the polychaete *Platynereis dumerilii* (*31*).

The homology of apical organs of cnidarians and bilaterians (planulozoan) has been proposed on the basis of the presence of ortholog transcription factors expressed in their apical organs (*Hox*, *NKx3*, *FoxJ1*, and *Irx*) and in apical domains (*Six3/6*, *FoxQ2*, and *rx*). The latter contributes to the specification of the apical pole of the larval body (*24*, *25*, *32*, *33*). In parallel, *Wnt* genes form a gradient at the oral end during early stages of development, and thus, the apical transcription factors are expressed in a *Wnt*-free zone (*24*, *32*, *34*). As these genes are expressed in similar domains in early-stage planulozoans, a possible interpretation is therefore that the last common ancestor of cnidarian and bilateria had an apical organ including an apical tuft (*24*). However, recent transcriptomic studies of cnidarian planulae have found a lack of apical ciliary tuft genes in scleractinian and schyphozoan cnidarians (*25*). This suggests that the common ancestor of cnidarians likely lacked a ciliary tuft (*25*).

[1]Michael Sars Centre, University of Bergen, Bergen, Norway. [2]University of Rostock, Institute of Biosciences, Rostock, Germany. [3]School of Biological and Medical Sciences, Oxford Brookes University, Oxford, UK.
*Corresponding author. Email: maike.kittelmann@brookes.ac.uk (M.K.); pawel.burkhardt@uib.no (P.B.)

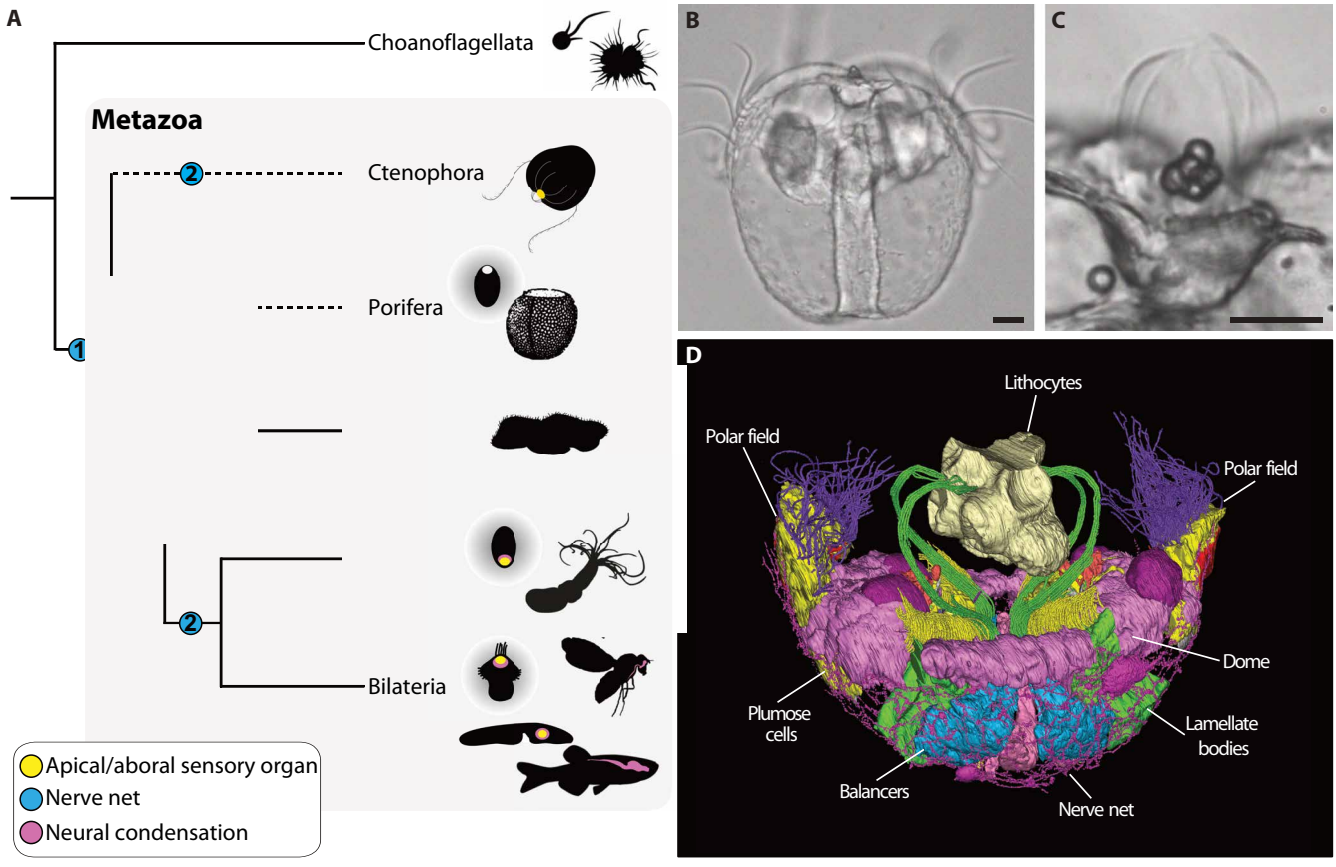

Fig. 1. The ctenophore aboral organ and the evolution of nervous system centralization. (**A**) Metazoan phylogeny and potential scenarios for the origin of neurons. The blue circle labeled "1" represents the hypothesis of a single neuronal origin. In contrast, the blue circles labeled "2" illustrate alternative hypotheses, suggesting that neurons may have evolved multiple times independently. Apical organs of cnidarian and bilaterian larvae are represented by yellow dots on the silhouettes and are associated with neural condensation (represented in pink). Neural condensation in adults is shown in pink. The aboral organ (AO) of ctenophores is represented by a yellow dot on the silhouette. The pigment ring that some sponge larvae have is shown in white. Silhouettes of Choanoflagellata, Placozoa, adult Cnidaria, and adult Bilateria were obtained and adapted from PhyloPic images (www.phylopic.org/). The *Conciliospongia anjiensis* silhouette is available under a CC BY 4.0 license (https://creativecommons.org/licenses/by/4.0/) and is provided by J. P. Botting, Y. Zhang, and L. A. Muir. (**B**). Phase contrast image of *M. leidyi* posthatching cydippid. The white box highlights the AO. (**C**) Higher magnification of the AO. (**D**) Three-dimensional (3D) reconstruction of the *M. leidyi* AO main cell types and enclosing nerve net. Scale bars, 30 μm.

In the ctenophore *Mnemiopsis leidyi*, *Wnt* genes are expressed later in development and show an inverse expression pattern confined to specific domains at the aboral pole (*35*). This suggests that *Wnt* genes specify precise aboral domains after the oral-aboral axis is established (*35*). In addition, there is evidence for a lineage-specific radiation of the *Six* genes in *M. leidyi*, whereas *Irx*, *Hox*, *Nkx3*, and *FGF* are lacking (*12*, *36*). Whether any of the few shared apical transcription factors have a conserved function in the AO of *M. leidyi* and whether the origin of apical integrative centers can be traced back to the last common ancestor of animals are not known (Fig. 1A). Here, we used volume electron microscopy to investigate the entire cellular composition and 3D architecture of the AO of the 1-day-old ctenophore *M. leidyi*. We uncovered diverse cell morphologies, including previously undescribed ones. We reveal an intimate association with the condensed SNN surrounding the AO, forming a potential multimodal circuit combining synaptic conduction and volume transmission. The expression patterns of key genes involved in anterior-posterior planulozoan axis formation and in the specification of apical organs suggest a complex evolutionary history of sensory aboral/apical integration centers.

RESULTS

Quantitative 3D cell type distribution of the ctenophore AO

We provide the first description of the 3D cellular architecture and cell numbers of an early posthatching ctenophore AO based on the investigation of five serial block-face scanning electron microscopy (SBFSEM) datasets (fig. S1 and movie S1). The segmentation of the nuclei ("*M. leidyi* RT" dataset; fig. S1) shows that the AO of the 1-day-old *M. leidyi* consists of almost 900 cells (Fig. 2, A to C, and fig. S2) and 17 distinct cell types (Fig. 2A and fig. S2). These include known cell types such as the balancers, the AO bridge, lamellate bodies, and plumose cells (*17*, *19*, *21*, *22*, *37*, *38*). Previously undescribed cell types encompass mono- or multiciliated and potentially secretory cells. We used the *M. leidyi* RT dataset (fig. S1) to assess the overall morphology of the AO. Additional datasets (fig. S1) to retrieve information about cellular shapes, subcellular features, integration with the nerve net, and the morphology of the nerve net itself were used (see below).

The statocyst consists of eight lithocytes suspended on four groups of balancers bearing sickle-shaped cilia (Fig. 2, D and E, and fig. S4)

A

Cell type	Cell number
Epithelial cells	301
Ciliated cells	233
Balancers (group of 4)	116
Dome cells	48
Polar field cells (group of 2)	48
Plumose cells (group of 2)	31
Ciliary groove cells (group of 4)	30
Polar field–associated cells (group of 2)	18
AO bridge cells	15
Lamellate bodies (group of 4)	15
Secretory cells C (group of 2)	13
Lithocytes	8
Secretory cells A	6
Secretory cells B	4
Large granular cells	4
Total	890

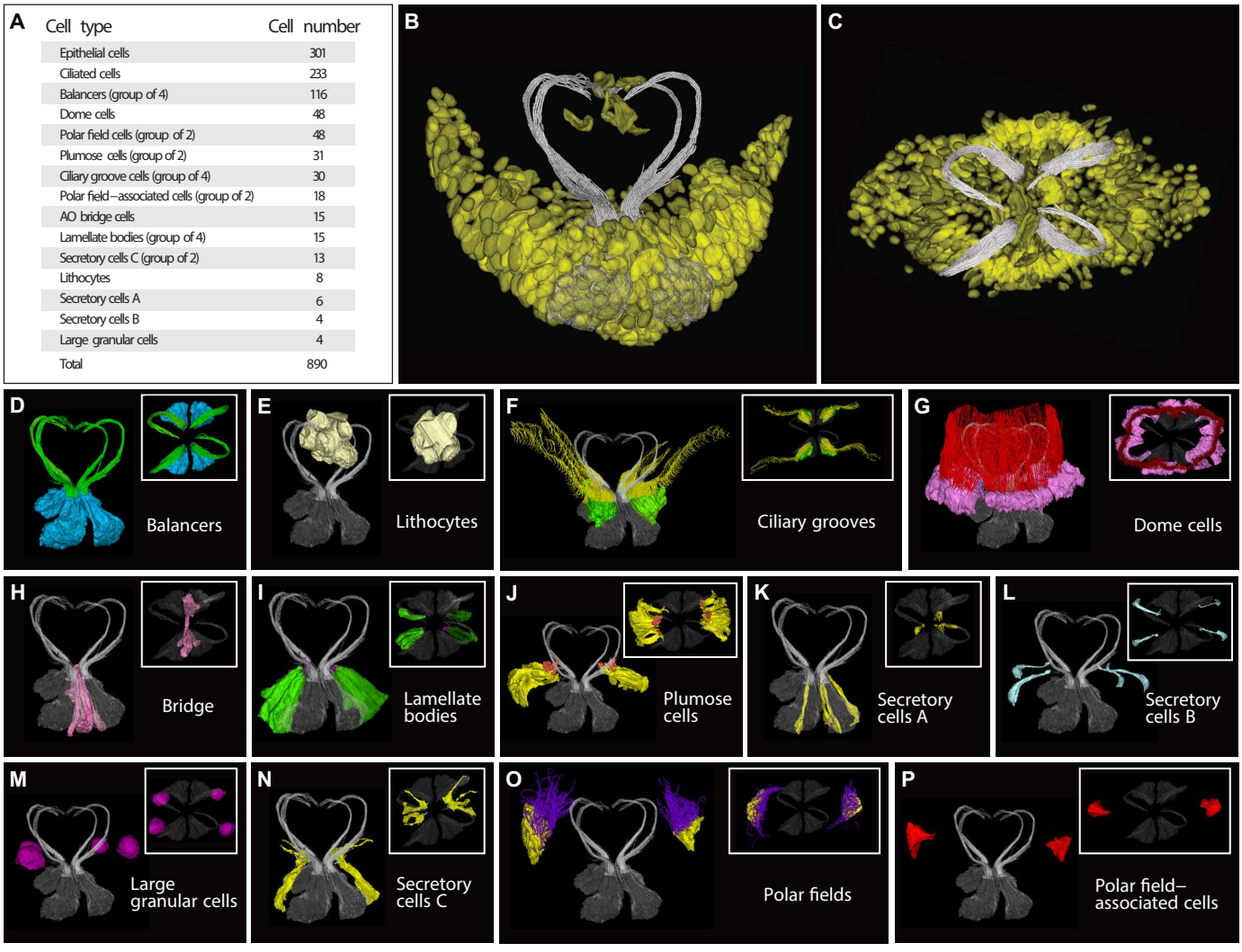

Fig. 2. High cell type diversity in the ctenophore AO. (**A**) Summary of *M. leidyi* AO cell types and cell numbers. The complete list of the 17 cell types is shown in fig. S2. (**B**) Lateral view of the AO nuclei (yellow). (**C**) Top view of the AO nuclei (yellow). Balancer cilia are gray in (B) and (C). (**D**) Balancer cell bodies (blue) and sickle-shaped cilia (green). (**E**) Lithocytes (light yellow). (**F**) Ciliated groove cell bodies (green) and cilia (yellow). (**G**) Dome cell bodies (pink) and dome cilia (red). (**H**) AO bridge cells (pink). (**I**) Lamellate bodies (green). (**J**) Plumose cell bodies (yellow) and cilia (orange). (**K**) Secretory cells A (yellow). (**L**) Secretory cells B (light blue). (**M**) Large granular cells (pink). (**N**) Secretory cells C (yellow). (**O**) Polar field cell bodies (yellow) and cilia (purple). (**P**) Polar field–associated cells (red). [(D) to (P)] Insets: Top views. [(E) to (P)] Balancers cells and cilia in gray.

(*22*, *39*). The lithocytes feature a large granule and a flattened peripheral nucleus (Fig. 2A and figs. S2 and S3B). Each group of balancers is formed by approximately 30 cells (Fig. 2A and fig. S2). Each balancer cell is equipped with a single motile cilium (fig. S3A) (*22*). The balancers are separated by the AO bridge, consisting of 15 cells (Fig. 2, A and H, and fig. S2), forming a continuous arch and oriented along the tentacular plane (fig. S3E) (*38*). The apical sides of each bridge cell are elongated and reach the contralateral group (fig. S3E). Ciliated grooves originate in proximity to the balancers and are organized into four groups, each consisting of two parallel rows of cells (Fig. 2F). Each group consists of seven to eight multiciliated cells (Fig. 2F and figs. S2 and S3C), yielding a total of 30 ciliated groove cells (Fig. 2A and fig. S2). The grooves extend beyond the dome of the AO, bifurcate, and connect to the comb rows (Fig. 2F and fig. S5) (*16*). The dome consists of 48 multiciliated cells (Fig. 2A and fig. S2) bearing long, nonmotile cilia that protect the AO environment (Fig. 2G and fig. S3D) (*22*). Four groups of one to six cells located in close proximity to the balancers correspond to the lamellate bodies (Fig. 2, A and I, and figs. S2 and S3F) (*21*). Multiple cilia originate basally and extend apically, reaching out to the extracellular space (fig. S3F). Their cytoplasm harbors numerous small dense-core and electron-lucent vesicles (see below). Cell types corresponding to the epithelial papillae or plumose cells (*17*, *19*, *20*) are arranged into two distal groups from the balancers and consist of 13 to 18 cells (Fig. 2, A and J, and fig. S2). The cell body is sigmoidal, and the cytoplasm exhibits a high density of electron-dense and electron-lucent vesicles (see below). Modified apical cilia show an overcoiled configuration (fig. S3G).

We found multiple putative secretory cells containing distinct types of vesicles. We identified six cells ("secretory cells A") neighboring the balancers and harboring apically polarized electron-lucent vesicles (Fig. 2K and figs. S2 and S3H). We reconstructed four cells ("secretory

cells B") containing small, polarized electron-dense vesicles and localized in proximity to the pressure cells (Fig. 2, A and L). The cell bodies are slender, the apical and basal poles are enlarged, and the nuclei are located basally (fig. S3I). We annotated 13 cells ("secretory cells C") distributed in two groups in proximity to the balancers, bearing long apical protrusions and small polarized electron-lucent vesicles (Fig. 2, A and N, and figs. S2 and S3K). Four large granular cells are located at the edge of the AO, close to the dome cells (Fig. 2, A and M, and fig. S2). The cell body is rounded, the nucleus is located basally, and several types of vesicles and reflective inclusions are densely interspersed within the cytoplasm (fig. S3J). Most of the remaining AO cells bear one or multiple cilia (table S1) and form a symmetrical pattern (fig. S6A). We identified about 200 mono-, bi-, and triciliated cells (Fig. 2A and figs. S2 and S3, L to N). These consist of elongated cell bodies, few mitochondria, and large nuclei (fig. S3, L to N). Most of these cells are monociliated cells (fig. S6, A and B), whereas bi- and triciliated cells are distributed in patches (fig. S6, B and C). Among the monociliated cells, we identified two single cells bearing longer cilia, situated among the ciliated grooves on the tentacular plane (fig. S3O). Live tubulin staining of cydippid indicates that these are motile cilia and bend laterally toward the ciliated grooves, establishing apparent contact (fig. S6, D and E, and movies S2 and S3). A cluster of monociliated cells ("bundle cells") is localized centrally, underneath the bridge (figs. 3P and S6F). We annotated 48 polar field cells (Fig. 2, A and O, and fig. S2) and 18 polar field–associated cells (Fig. 2, A and P, and fig. S2) distributed in two groups on the outer side of the dome (Fig. 1D). The polar field cells are multiciliated cells equipped with long motile cilia (fig. S3Q), whereas the polar field–associated cells are nonciliated, displaying thin apical protrusions (fig. S3R). Last, we annotated about 300 round-shaped and elongated epithelial cells (Fig. 2A and figs. S2 and S3, S and T) scattered among other AO cells (table S1).

Condensation of the subepithelial nerve net around the AO

We traced neural cell bodies and neurites of the SNN near the AO and consistently observed a syncytial architecture with interconnected neurites extending from the neural cell bodies as previously described (Fig. 3A) (*18*). The AO-adjacent nerve net consists of four symmetrically distributed neural cell bodies (Fig. 3A). The nerve net encases the AO, and the neurites are situated close to the basal poles of the cells (Fig. 3A, top and bottom insets). The morphology of the

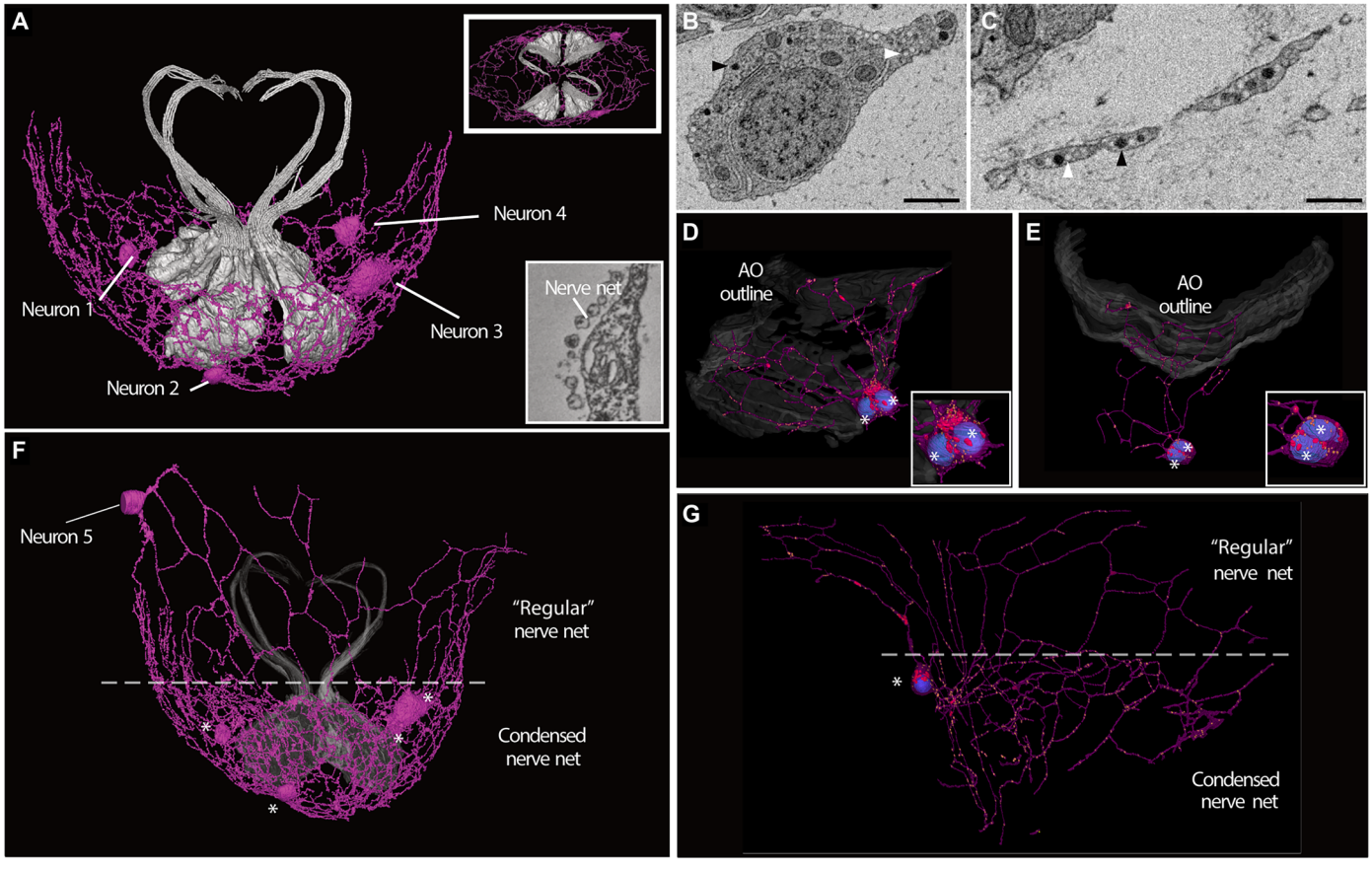

Fig. 3. Condensation of the nerve net encasing the AO. (**A**) 3D reconstruction reveals the syncytial architecture of the AO nerve net (pink). Four nerve net cell bodies are interconnected by neurites. The relative position to the balancer cells (gray) is shown (top inset: top view of the balancer cells and the AO nerve net; bottom inset: ultrastructure of the "pearls-on-a-string" morphology). (**B**) SBFSEM cross section of a nerve net cell body, including electron-dense (black arrowhead) and electron-lucent vesicles (white arrowhead). (**C**) SBFSEM cross section of a neurite including electron-dense (black arrowhead) and electron-lucent vesicles (white arrowhead). (**D** and **E**) 3D reconstruction of nerve net cell bodies containing two nuclei (white asterisks). The neurites extend toward the AO cells (AO outline in gray). (**F**) The nerve net above the dashed line extends toward the neighboring epithelial cells and shows characteristic, large polygons, including an additional cell body (neuron 5). The nerve net below the dashed line, which includes four cell bodies (asterisks), shows compact, small polygons. (**G**) 3D reconstruction of high-pressure frozen tissue confirms condensation of the nerve net encasing the AO. Nerve net cell body (asterisk: nerve net cell body; blue: nucleus and neurites extending from it (pink); yellow: electron-dense vesicles; red: mitochondria). Scale bars, 1 μm.

neurites shows the typical pearl-on-a-string structure (Fig. 3A, bottom inset) and is overall consistent with that of the subepithelial nerve net (Fig. 3, B and C) (*18*). However, we observed some neurites exhibiting slightly thicker and continuous morphologies, interspersed with the pearl-on-a-string structures (Fig. 3C). Similar to the subepithelial nerve net, the neural cell bodies and neurites contain dense-core and electron-lucent vesicles (Fig. 3, B and C, and figs. S3U and S7). We observed sheets of endoplasmic reticulum (ER) embedded in the cytoplasm of these cell bodies, suggesting a higher synthetic activity in this cellular compartment. This is consistent across datasets (Fig. 3 and fig. S7). The datasets of "animal 4" and "animal 5" (fig. S1) revealed neural cell bodies containing two nuclei (Fig. 3, D and E, insets), although the ultrastructure is similar to mononucleated cell bodies, including vesicles and ER membranes (Fig. 3, D and E). Extended reconstruction of the SNN toward the epithelium flanking the AO revealed a change in the SNN architecture. While the syncytium is maintained, we observed a substantial increase in neurite density in close proximity to the AO cells. Here, neurites are densely packed and highly interconnected, and the number of polygons per SNN area increases. We define this configuration as "condensed" SNN. This is characterized by the presence of denser polygons in contrast to the SNN (Fig. 3, F and G). The condensed and "regular" SNN configurations are observed consistently across datasets and fixation techniques (Fig. 3, F and G, and fig. S1).

Signal conduction routes in the AO

Our 3D reconstructions revealed neurite projections that extend from SNN neurons to form synaptic contacts onto two effector cells, the balancers and the bridge cells (Fig. 4). Multiple synapses were detected at the base of the balancer cells, consistent with previous observations (*40*), while some neurites extended among the balancer cells and reached toward the apical poles of the cell complex (Fig. 4, A and B). The neurites extend from a proximal neural cell body and envelop the group of balancers (Fig. 4, C and D). A similar multisynaptic configuration is detected at the bridge cells, although the neurites are not intertwined within the cell group (Fig. 4, E and F). The synaptic contacts are characterized by the typical synaptic triad, including a mitochondrion, ER, and vesicles (Fig. 4G) (*37*, *40*). Distinct and specialized cell types include the lamellate bodies, plumose cells, and putative secretory cells (Fig. 4, H to L). These are equipped with numerous nonsynaptic electron-dense and electron-lucent vesicles (Fig. 4, H to K). The lamellate bodies harbor small electron-lucent vesicles spanning the length of the cell body and medially polarized small electron-dense vesicles (Fig. 4H). The plumose cells' cytoplasm is heavily loaded with large electron-dense vesicles, whereas electron-lucent vesicles polarize at the apical pole (Fig. 4I). In contrast, the secretory cells contain only one type of nonsynaptic vesicle (Fig. 4, J to L). Secretory cells A and C contain nonsynaptic electron-lucent vesicles (Fig. 4, J and L). In both cases, the vesicles are polarized apically. Conversely, secretory cells B harbor only electron-dense vesicles, which show a medial-basal polarization (Fig. 4K). These cell types may contribute to an alternative nonsynaptic route for signal conduction in the AO through volume transmission (Fig. 4M).

AO and apical domain genes in *M. leidyi*

We investigated the expression of genes involved in the specification of the planulozoan apical organ and apical domain. Specifically, we searched for orthologs of the *Six3/6*, *FoxQ2*, *rx*, and *FoxJ1* transcription factors in *M. leidyi*. Using orthology inference analysis and gene phylogeny, we identified two genes, *ML082610a* and *ML01466a*, sharing a common ancestor with the *Six3/6* clade (table S2 and fig. S9). These genes ("*MlSix3/6A*" and "*MlSix3/6B*"; fig. S8) show a close relationship, and their grouping in the phylogenetic tree suggests a possible lineage-specific evolutionary event, consistent with previous studies (fig. S9) (*36*). In the 1-day-old *M. leidyi*, *MlSix3/6A* is expressed in the epithelium along the comb rows, and *MlSix3/6B* is expressed in the pharynx area and large, isolated cells on the outer epithelium of the tentacle bulb and the distal pharynx area or mouth (fig. S8B). The temporal expression pattern shows that both genes start to be expressed around 8 to 11 hours postfertilization (fig. S8A) (*41*). An ortholog of the Forkhead transcription factor *FoxQ2* was identified (fig. S10); however, the expression in the 1-day-old *M. leidyi* could not be detected. Our analysis revealed an orthogroup containing several homeobox domain–containing genes, including the *HBN* gene of *Drosophila melanogaster*, other paired-type homeobox family members, and three *M. leidyi* genes (table S2). A gene phylogeny encompassing paired-type homeobox family genes and the three ones identified from *M. leidyi* was computed (fig. S11). Our analysis revealed that *ML213986a* ("*Mlrx-like*") is closely related to *rx* genes of other species (fig. S10). The expression of *Mlrx-like* is detected in the proximal half region of the tentacle bulbs, forming a semicircular pattern in the 1-day-old *M. leidyi* (fig. S8B). Temporal expression data show that *Mlrx-like* starts to be expressed around gastrulation (fig. S8A) (*41*). We additionally focused our gene orthology analysis on the Forkhead transcription factor, *FoxJ1*. Our analysis revealed orthology of *ML23712a* ("*MlFoxJ1*") with other genes belonging to the *FoxJ1* family (table S2 and fig. S10). In the 1-day-old *M. leidyi*, *MlFoxJ1* is expressed in the AO in four dense symmetrical patches, and a punctate signal can be detected in between the dense areas and in the ciliated groove area connecting to the comb rows (Fig. 5, A, B, C, and E). A well-defined expression of *MlFoxJ1* is detected along the comb rows (Fig. 5, B, D, and E) that develop around 9 hours after fertilization (*42*). Temporal expression data indicate that *MlFoxJ1* starts to be expressed around gastrulation (fig. S8A).

DISCUSSION

AO complexity in ctenophores

The assemblage of complex integrative centers likely marked the expansion of the pelagic phase in organisms with larger multicellular bodies. The enhanced capability of interpreting the environment on a large scale allowed early animals to process inputs and react rapidly (*3*, *4*). Since its first description as a sensory organ by R. Hertwig in 1880, several studies have aimed to understand the unique morphology and behavioral modulation of the ctenophore AO (*16*, *19*, *37*–*39*). Our volume electron microscopy–based 3D reconstruction of a 1-day-old *M. leidyi* reveals the spatial organization of the cellular diversity within the AO. We show that the AO consists of about 900 cells, distributed into 17 cell types (including previously described balancers, bridge cells, plumose cells, and lamellate bodies). In addition, our study describes putative secretory cells, ciliated cells, epithelial cells, dome, polar fields, and polar-field–associated cells and a previously undescribed association with a condensed part of the SNN. Moreover, we report previously unidentified types of several secretory and ciliated cells. Distinct vesicle populations in secretory cells suggest discrete signals and signaling pathways (see below), whereas we hypothesize that, so far, undescribed ciliated cells contribute to the overall sensory capability of

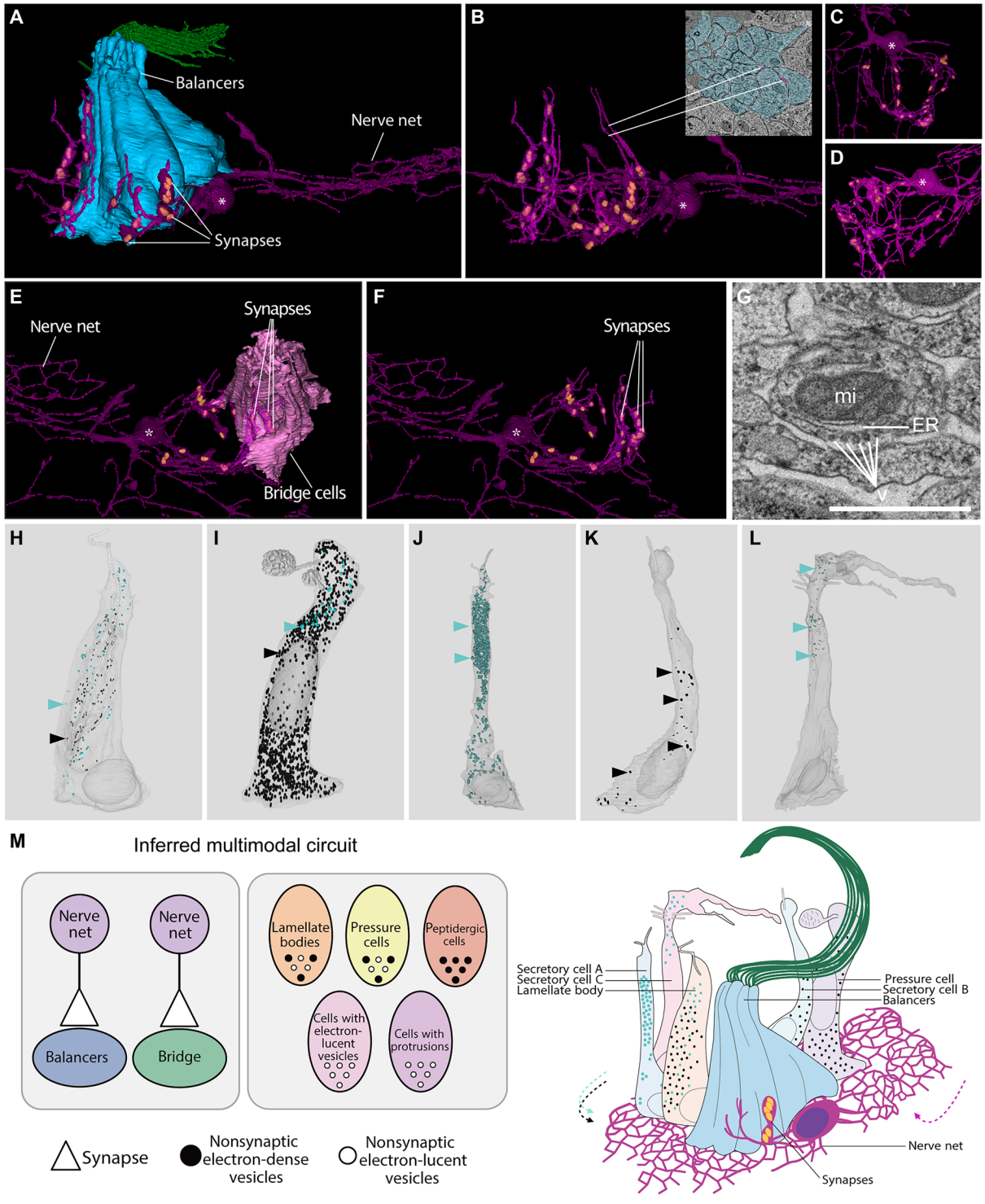

Fig. 4. Inferred multimodal neuronal architecture used by the ctenophore AO. (**A**) 3D reconstruction reveals direct synaptic contacts between nerve net neurons and balancers. Blue: balancers; green: cilia. (**B**) Long neurites containing multiple synapses are intertwined with the balancers' cell bodies. Inset: SBFSEM cross section. Blue: balancers; pink: nerve net neurites. (**C**) Top view and (**D**) lateral view of the nerve net associated with balancers. (**E**) 3D reconstruction reveals direct synaptic contacts between nerve net neurons and bridge cells. (**F**) Several synapses form connections to bridge the cell bodies. [(A) to (F)] Asterisks: nerve net cell bodies; yellow: mitochondria. (**G**) Transmission electron microscopy (TEM) cross section of a synaptic triad, including a mitochondrion (mi), ER, and synaptic vesicles (v). (**H**) 3D reconstruction of a lamellate body. (**I**) 3D reconstruction of plumose cells. (**J**) 3D reconstruction of secretory cell A. (**K**) 3D reconstruction of secretory cell B. (**L**) 3D reconstruction of secretory cell C. Light blue dots and arrowheads: nonsynaptic electron-lucent vesicles; black dots and arrowheads: electron-dense vesicles. (**M**) Inferred AO circuitry and circuit model indicating synaptic contacts and potential volume transmission. Scale bar, 1 μm.

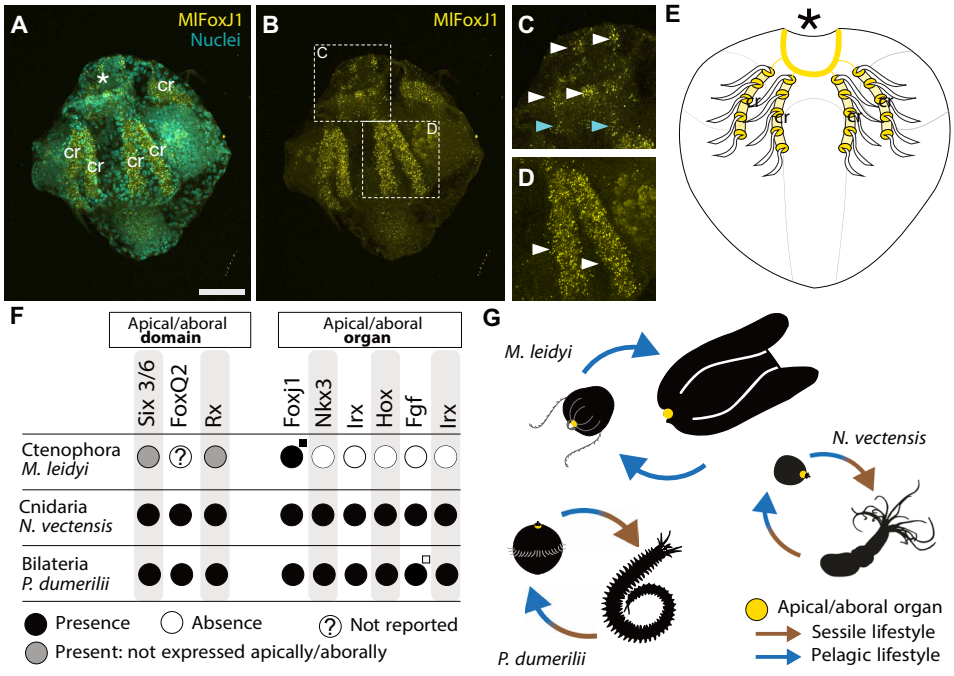

Fig. 5. Complex evolutionary history of aboral integration centers. (**A**) Expression of *MlFoxJ1* (yellow) and nuclei (cyan) in a 1-day-old cydippid of *M. leidyi*. (**B**) *MlFoxJ1* expression in the AO and the comb rows. (**C**) Higher magnification of the AO. White arrowheads indicate *MlFoxJ1* expression. Cyan arrowheads indicate expression in the ciliated grooves. (**D**) Higher magnification of the comb rows. White arrowheads indicate *MlFoxJ1* expression. (**E**) Schematics of *MlFoxJ1* expression. Asterisks: AO; cr: comb rows. Scale bar, 50 μm. (**F**) Presence-absence table of transcription factors contributing to the apical/aboral domain and organ specification across ctenophores, cnidarians, and bilaterian using *M. leidyi*, *N. vectensis*, and *P. dumerilii* as reference species. Black dots indicate presence in the genome and in the apical/aboral domain or organ. White dots indicate absence in the genome. Gray dots indicate presence in the genome but lack of expression in the apical/aboral domain or organ. White dots with question marks indicate lack of reported expression. The small black square indicates the additional expression of *MlFoxJ1* in comb rows; the small white square indicates expression of the Fgf receptor only. (**G**) Simplified life cycle of *M. leidyi*, *N. vectensis*, and *P. dumerilii*. Yellow dots indicate the apical/AOs. *M. leidyi* remains pelagic, and the AO is found at early and later stages. *N. vectensis* transitions from a pelagic planula to a sessile polyp. *P. dumerilii* metamorphoses from a pelagic larva to a sessile adult worm that becomes pelagic again to mate (pelagic adult form not shown). Silhouettes of adult *M. leidyi*, adult *N. vectensis*, and adult *P. dumerilii* were obtained from www.phylopic.org/. The silhouette of *P. dumerilii* is available under the CC BY-NC-SA 3.0 license (https://creativecommons.org/licenses/by-nc-sa/3.0/), and it is provided by B. Duygu Özpolat.

the AO. Together, the presence of multiple and distinctive cell types identifies the AO as a complex sensory organ capable of processing and integrating diverse sensory signals. A direct connection with the locomotory system (i.e., the comb rows) establishes the AO as an essential system for input processing and behavioral coordination.

A condensed SNN is associated with the AO

The AO is enclosed by a condensed section of the SNN (Fig. 3). The cytoplasm of the SNN cell bodies of this section is enriched with ER sheets compared to previous findings (fig. S7) (*18*), indicating high metabolic activity. In addition, we found SNN cell bodies with multiple nuclei in slightly older animals (Fig. 3), which could result from karyokinesis. These findings are consistent with an expansion in the number of neural cell bodies and remodeling of the SNN in older animals, as shown by reconstruction of the neurons surrounding the AO in the 5-day-old cydippid (*43*). The condensed architecture points toward the necessity to enhance neuronal wiring in an area of increased signaling activity. Alternatively, although not in contrast, a hierarchical mode of signaling mechanisms could exist, whereby the input, processing, and output take place in the AO compartment and involve the concerted participation of specialized cells and the SNN. The output likely propagates to the rest of the body, yielding behavioral modulation [e.g., change of the swimming pattern in relation to light intensities (*16*, *44*)].

Nonetheless, we cannot exclude the possibility that the cellular context influences neurite patterning and, consequently, the observed condensation. The AO region is densely populated by columnar cells, whereas the surrounding epithelium consists of larger, flattened cells. If neurite organization is guided by cellular boundaries, then this could produce a more compact architecture with smaller polygons aligned with the AO and larger polygons corresponding to the epithelial cells. To assess whether this condensed nerve net contributes to signal conduction, a receptor density map (e.g., for G protein–coupled receptors and ion channels) together with functional validation of signal transmission in the AO—such as through calcium imaging—will be required.

An emerging multimodal circuit

We report synaptic connections from the SNN onto the balancers and the bridge. Previously reported synaptic contacts from the SNN onto the ciliated grooves (*45*) and comb cells (*18*) support the possibility of a comprehensive neural circuit that coordinates swimming responses (*16*, *22*, *46*). Alternatively, nerve net synapses contacting the bridge cells could form a different subcircuit involved in prey-capture behaviors (*38*). Additional synaptic contacts onto lamellate bodies and secretory cells have previously been reported for adult ctenophores (*20*). These contacts were not present in our data, indicating that lamellate bodies, and possibly other cell types, become

wired into one or multiple circuits later in development, reflecting an even greater behavioral coordination. In any case, synaptic conduction constitutes a defined pathway for signal propagation toward the AO. However, the propagation via volume transmission appears to be functioning simultaneously. Lamellate bodies, plumose cells, and other secretory cells harbor highly polarized, electron-dense, and electron-lucent vesicles (Fig. 4) and could serve as key players in volume transmission (Fig. 4L). The occurrence of volume transmission in the AO is supported by the expression of neuropeptides and their effect on swimming behaviors [e.g., ML065755 (*45*)]. The potential coexistence of synaptic and volume transmission suggests that ctenophores use a multimodal circuit to connect the nervous system and cellular components in the AO (Fig. 4L). To further dissect neural signaling in ctenophores, a better understanding of the molecular signature of the chemical synapses and a map of neuropeptide-receptor interactions is required.

Evolutionary origin of sensory complexes

Molecular and morphological studies suggested the homology of bilaterian apical organs (*29*, *47*). Comparative analysis of transcription factors involved in the development of the apical region and the apical organ across cnidarian and bilaterian revealed conserved expression patterns, which were used to propose the homology of apical organs within planulozoans (*24*). This further suggests that the planulozoan ancestor may have had an apical organ and an apical tuft (*24*). However, comparative transcriptomics analysis across cnidarian planulae revealed that some lineages lack the transcriptional signature of the apical ciliary tuft along the tuft itself, questioning the proposed homology of the ciliary tufts (*25*). How the ctenophore AO fits within the evolutionary history of apical sensory integration centers remains controversial, due to its distinct morphology (fully illustrated in this study) and the lack of conserved gene expression (*3*, *12*, *35*, *36*).

The transcription factor *MlFoxJ1* is the sole gene commonly present in *M. leidyi* and in apical organs of other metazoans (Fig. 5F). *FoxJ1* transcription factor orthologs are expressed in the apical organ of *M. leidyi*, early pigment-ring–forming embryos of *Amphimedon queenslandica* (*48*), the apical region of *N. vectensis* (*32*), and *P. dumerilii* larvae (*24*). The occurrence of *FoxJ1* predates the evolution of animals. It is down-regulated in cRFXa mutants with aberrant ciliogenesis, although direct perturbation of *FoxJ1* has no effect on ciliogenesis in the choanoflagellate *Salpingoeca rosetta* (*49*). This indicates not only its ancestral involvement in the development of ciliated structures but also its tight regulation by other factors. The expression of *MlFoxJ1* in both the AO and the comb rows in *M. leidyi* suggests that the involvement in the development of ciliary structures is conserved. However, we cannot determine whether *MlFoxJ1* plays a role in the patterning of ciliated structures or belongs to a terminal selector module that has been redeployed in the comb rows and the AO of ctenophores. Increased taxon sampling of early-branching animals and further investigation of ciliary gene regulatory networks across species will clarify how the patterning of ciliated sensory complexes evolved.

It is also important to consider that cnidarian and bilaterian AOs are transient organs, only found at early stages, whereas the ctenophore AO is a nontransient structure present in early and later stages in pelagic ctenophores (Fig. 5G) (*19*, *23*). Ctenophores are direct developers and can reproduce a few weeks after hatching (*15*). The presence of the AO throughout the ctenophore life suggests a fundamental role in all life phases, contrary to cnidarian and bilaterian larval AO. The molecular pathways underlying the development and the specification of the ctenophore AO appear to be uniquely evolved in this group and pose a challenge to disentangle the evolution of integrative centers. Developmental cell atlases of *M. leidyi* will provide a basis to investigate gene expression in early stages and potentially resolve gene regulatory networks in ctenophores. We interpret the ctenophore AO as an unparalleled sensory structure that likely evolved independently in the ctenophore lineage and is tightly linked to the direct-developing pelagic life cycle (Fig. 5G). This is supported by the unique cell type composition, the distinct neuronal integration, the role in behavior, and the lack of conserved transcription factor expression.

MATERIALS AND METHODS

Animal husbandry

For electron microscopy, *M. leidyi* cydippids were maintained in 300-ml glass beakers and fed daily with *Brachionus*, as previously described (*50*, *51*). For hybridization chain reaction (HCR), adults of *M. leidyi* were maintained in 25 liters of Kreisels and fed daily with *Brachionus* and *Artemia*. In both cases, animals were maintained under a 17-hour/7-hour light-to-dark cycle (*50*, *51*). Following 7 hours of darkness, adults were transferred to 300-ml beakers and allowed to release gametes. Fertilized eggs were transferred to 1 liter of glass beakers with aeration and incubated until fixation. Neither animal health nor animal welfare regulations apply to ctenophores under the Norwegian Animal Welfare Act and the UK Animals in Scientific Procedures Act 1986 (www.regjeringen.no/en/documents/animal-welfare-act/id571188/ and www.legislation.gov.uk/ukpga/1986/14/section/1).

Electron microscopy sample preparation

Fixation by high-pressure freezing (HPF) and freeze substitution (FS) was previously described (*45*). Briefly, *M. leidyi* cydippids were frozen in 20% bovine serum albumin in natural seawater in 0.2-mm aluminum planchettes in a Bal-Tec 10 High Pressure Freezer. Samples were placed in cryotubes with frozen 0.1% uranyl acetate + 1% osmium tetroxide in liquid nitrogen and transferred to an RMS FS machine: 20 hours at −90°C, 21 hours from −90° to −20°C, 24 hours at −20°C, 5 hours from −20° to 4°C, and 30 min from 4° to 20°C. At room temperature (RT), samples were washed in acetone and incubated in 1% tannic acid in acetone for 2 hours; washed in acetone; incubated for 2 hours in 1% osmium tetroxide; washed in acetone and infiltrated in a series of 10, 30, 50, and 70% TAAB 812 hard Epoxy resin for at least 3 hours each or overnight; and then infiltrated 3× in fresh 100% TAAB 812 hard Epoxy resin for at least 4 hours each or overnight at 4°C. Cydippids were then embedded in fresh resin and polymerized at 70°C for at least 24 hours.

For chemical fixation, *M. leidyi* cydippids were fixed in 2% glutaraldehyde and 2.5% paraformaldehyde in 0.1 M NaCac (pH 7), made up in 27 parts per thousand (ppt) seawater, gently rocking for 3 hours at 4°C. Cydippids were then washed 3× in seawater, then stained with 2% osmium (aqueous) overnight at 4°C, washed 3× in water, stained with 1% tannic acid (aq.) for 4 hours at 25°C, washed 3× in water, stained with 1% osmium overnight at 4°C, washed 3× in water, stained with 2% uranyl acetate (aq.) for 2 hours, washed 3× in water, and dehydrated in a series of 10, 30, and 50% EtOH for 45 min each. After overnight 70% EtOH incubation, they were placed in 4× fresh 100% ethanol for 4 hours or overnight each, lastly infiltrated in a series of 10, 30, 50, and 70% for at least 3 hours each, and then infiltrated with 812 Epoxy resin as described above.

SBFSEM

For SBFSEM, *M. leidyi* cydippids were prepared as previously described (*45*). Briefly, samples were glued onto SBFSEM stubs with conductive Epoxy resin (Chemtronics, Hoofddorp, Netherlands), trimmed with a diamond trimming knife, and sputter coated with 20 nm of gold. Images were collected with a Merlin Compact SEM (Zeiss, Cambridge, UK) with the Gatan 3View system and Gatan OnPoint BSD and Focal Charge Compensation (100%) with a 20-µm aperture, at 1.8 kV and a 1-µs pixel time. Pixel size of raw data is specified in fig. S1 for each dataset. The datasets are available here: https://doi.org/10.6084/m9.figshare.29314115.v1.

SBFSEM datasets overview, segmentation, and 3D reconstruction

We generated five SBFSEM datasets using chemical fixation (*M. leidyi* RT; fig. S1) and HPF ("*M. leidyi* HPF1," "*M. leidyi* HPF2," "*M. leidyi* HPF3," and "*M. leidyi* HPF4"; fig. S1). SBFSEM sections were imported into Fiji (*52*) and aligned to generate Z-stacks using default parameters, as previously described (*18*, *45*). Stacks were imported into TrakEM2 (*53*), and segmentation of organelles, cilia, and nerve net was performed manually. Segmentation of nuclei and membranes was performed semiautomatically using the function "interpolate gaps," where possible. Meshes were visualized with 3D Viewer (*54*), rendered at a resolution of 1 to 3 for the nerve net, of 5 for single cells, and 10 for composites. Meshes were smoothed by a factor of 5 to 10, and small vesicles were not smoothed. We exploited "animal 1" dataset the most, as it contains full coverage of the AO. We leveraged the remaining datasets to examine details of the subcellular features and the nerve net architecture.

Fixation of specimens for whole-mount in situ hybridization (HCR)

Cydippids of *M. leidyi* were collected after 24 hours postfertilization and fixed as previously described by Mitchell *et al.* (*55*) with the following modifications. Briefly, animals were transferred into glass vials containing 2.5 ml of artificial seawater (ASW) and rapidly relaxed by adding 500 µl of 1 M $MgCl_2$. Fixation was conducted with 16% ice-cold Rain-X in ASW (27 ppt; pH 8.2) for 20 min under constant rotation. Cydippids were postfixed in 3.7% ice-cold formaldehyde solution in ASW for 20 min at 4°C under constant gentle rotation. Following fixation, animals were washed three times in phosphate-buffered saline [PBS; 137 mM NaCl, 2.68 mM KCl, 10.14 mM Na_2HPO_4, and 1.76 mM KH_2PO_4 (pH 7.4)] with 0.1% Tween 20 (Sigma-Aldrich) and dehydrated stepwise in methanol. Fixed specimens were stored at −20°C and rehydrated stepwise in PBS–0.1% Tween 20 before proceeding with HCR.

Whole-mount in situ hybridization (HCR)

In situ HCR v3.0 with split initiator probes was performed using amplifiers and buffers obtained from Molecular Instruments (www.molecularinstruments.com) (*56*). Probes for HCR were designed with the insitu_probe_generator custom script (*57*). Probe sets were ordered from Integrated DNA Technologies (https://eu.idtdna.com). Rehydrated samples were incubated in the Probe Hybridization buffer (Molecular Instruments) for 1 hour at 37°C. Probes were used at a concentration of 16 nM and incubated overnight at 37°C. Following incubation, samples were washed four times in Probe Wash buffer (Molecular Instruments) for 15 min at 37°C and then five times in 5× SSC buffer (SSC 20×; 0.75 M sodium chloride and 0.075 M sodium citrate, Thermo Fisher Scientific) containing 0.1% Tween 20 (Sigma-Aldrich) for 5 min at RT. Samples were preamplified in Amplification buffer for 30 min at RT. Hairpins were used at a concentration of 60 nM, heated in a polymerase chain reaction thermocycler for 90 s at 95°C, and allowed to cool down for 30 min at RT in the dark. Hairpins were then mixed with the Amplification buffer, and solutions were added to the samples and incubated overnight at RT in the dark. Following amplification, samples were washed twice in 5× SSCT (5x SSC with 0.1% Tween 20) for 5 min, followed by nuclear staining using 1:2000 Hoechst 33342 (10 mg/ml; Thermo Fisher Scientific) in 5× SSCT for 30 min at RT. Last, samples were washed three times in 5× SSC and mounted in SlowFade Glass soft-set antifade mounting medium.

Live staining

Recently hatched cydippids were washed with ASW and incubated with 1 µM SiR tubulin (Cytoskeleton Inc., CY-SC002) in ASW overnight at 18°C. The animals were then washed three times with ASW before mounting on glass bottom dishes (MatTek, P35G-1.5-10-C) in 0.5% low-melt agarose (catalog no. CR-6351.5) in ASW containing 100 nM SiR tubulin.

Confocal imaging and image analysis

Images of fixed specimens and videos of live animals were acquired with an Olympus FV3000 confocal laser scanning microscope, and Z-stack maximum intensity projections were obtained with Fiji (*52*). Contrast and brightness of the images were adjusted by refining the contrast and the brightness of the maximum projections to improve the visualization of the gene expression.

Gene orthology

Search for clusters of orthologous genes was performed with Broccoli 1.2 (*58*) using the maximum likelihood algorithm for steps 1, 2, and 3. We used available proteomes for *Homo sapiens* (UP000005640_9606), *D. melanogaster* (UP000000803_7227), *Caenorhabditis elegans* (UP000001940_6239), *N. vectensis* (UP000001593_45351), *Mus musculus* (UP000000589_10090), *Danio rerio* (UP000000437_7955), *P. dumerilii* (901 annotated proteins), and *M. leidyi* (https://research.nhgri.nih.gov/mnemiopsis/). We recovered four orthogroups, each containing *MlSix3/6A and B*, *MlFoxq2*, *MlFoxJ1*, and *Mlrx-like* (table S2). To validate our orthogroups, we performed gene phylogenies. We compiled lists of protein families from the sample of species used in Broccoli, including only full-length proteins. The list used to validate the orthogroup containing *Mlrx-like* also included proteins from *Strongylocentrotus purpuratus.* We generated sequence alignments using MUSCLE 5.3 (*59*) with default parameters. Alignments were cleaned using trimAl 1.5 (*60*) with default parameters. Gene phylogenetic trees were built using IQ-TREE 2 2.4 (*61*) using the MFP option, allowing for the best substitution model to be selected. Phylogenetic trees including *MlSix3/6A*, *MlSix3/6B*, *MlFoxQ2*, *MlFoxJ1*, and *Mlrx-like* are available in figs. S9 to S11.

Supplementary Materials

The PDF file includes:

Figs. S1 to S11
Legends for tables S1 and S2
Legends for movies S1 to S3

Other Supplementary Material for this manuscript includes the following:

Tables S1 and S2
Movies S1 to S3

REFERENCES

1. G. E. Budd, S. Jensen, The origin of the animals and a 'Savannah' hypothesis for early bilaterian evolution: Early evolution of the animals. *Biol. Rev.* **92**, 446–473 (2017).
2. P. Burkhardt, G. Jékely, Evolution of synapses and neurotransmitter systems: The divide-and-conquer model for early neural cell-type evolution. *Curr. Opin. Neurobiol.* **71**, 127–138 (2021).
3. D. Arendt, M. A. Tosches, H. Marlow, From nerve net to nerve ring, nerve cord and brain-evolution of the nervous system. *Nat. Rev. Neurosci.* **17**, 61–72 (2016).
4. P. Martinez, S. G. Sprecher, Of circuits and brains: The origin and diversification of neural architectures. *Front. Ecol. Evol.* **8**, 82 (2020).
5. A. K. Redmond, A. McLysaght, Evidence for sponges as sister to all other animals from partitioned phylogenomics with mixture models and recoding. *Nat. Commun.* **12**, 1783 (2021).
6. P. Simion, H. Philippe, D. Baurain, M. Jager, D. J. Richter, A. Di Franco, B. Roure, N. Satoh, É. Quéinnec, A. Ereskovsky, P. Lapébie, E. Corre, F. Delsuc, N. King, G. Wörheide, M. Manuel, A large and consistent phylogenomic dataset supports sponges as the sister group to all other animals. *Curr. Biol.* **27**, 958–967 (2017).
7. D. Pisani, W. Pett, M. Dohrmann, R. Feuda, O. Rota-Stabelli, H. Philippe, N. Lartillot, G. Wörheide, Genomic data do not support comb jellies as the sister group to all other animals. *Proc. Natl. Acad. Sci. U.S.A.* **112**, 15402–15407 (2015).
8. J. L. Steenwyk, N. King, The promise and pitfalls of synteny in phylogenomics. *PLOS Biol.* **22**, e3002632 (2024).
9. R. R. Copley, Sponges, ctenophores, and the statistical significance of syntenies. *Mol. Biol. Evol.* **42**, msaf321 (2025).
10. C. W. Dunn, A. Hejnol, D. Q. Matus, K. Pang, W. E. Browne, S. A. Smith, E. Seaver, G. W. Rouse, M. Obst, G. D. Edgecombe, M. V. Sørensen, S. H. D. Haddock, A. Schmidt-Rhaesa, A. Okusu, R. M. Kristensen, W. C. Wheeler, M. Q. Martindale, G. Giribet, Broad phylogenomic sampling improves resolution of the animal tree of life. *Nature* **452**, 745–749 (2008).
11. L. L. Moroz, K. M. Kocot, M. R. Citarella, S. Dosung, T. P. Norekian, I. S. Povolotskaya, A. P. Grigorenko, C. Dailey, E. Berezikov, K. M. Buckley, A. Ptitsyn, D. Reshetov, K. Mukherjee, T. P. Moroz, Y. Bobkova, F. Yu, V. V. Kapitonov, J. Jurka, Y. V. Bobkov, J. J. Swore, D. O. Girardo, A. Fodor, F. Gusev, R. Sanford, R. Bruders, E. Kittler, C. E. Mills, J. P. Rast, R. Derelle, V. V. Solovyev, F. A. Kondrashov, B. J. Swalla, J. V. Sweedler, E. I. Rogaev, K. M. Halanych, A. B. Kohn, The ctenophore genome and the evolutionary origins of neural systems. *Nature* **510**, 109–114 (2014).
12. J. F. Ryan, K. Pang, C. E. Schnitzler, A. D. Nguyen, R. T. Moreland, D. K. Simmons, B. J. Koch, W. R. Francis, P. Havlak, S. A. Smith, N. H. Putnam, S. H. D. Haddock, C. W. Dunn, T. G. Wolfsberg, J. C. Mullikin, M. Q. Martindale, A. D. Baxevanis, The genome of the ctenophore *Mnemiopsis leidyi* and its implications for cell type evolution. *Science* **342**, 1242592 (2013).
13. D. T. Schultz, S. H. D. Haddock, J. V. Bredeson, R. E. Green, O. Simakov, D. S. Rokhsar, Ancient gene linkages support ctenophores as sister to other animals. *Nature* **618**, 110–117 (2023).
14. C. W. Dunn, S. P. Leys, S. H. D. Haddock, The hidden biology of sponges and ctenophores. *Trends Ecol. Evol.* **30**, 282–291 (2015).
15. A. Edgar, J. M. Ponciano, M. Q. Martindale, Ctenophores are direct developers that reproduce continuously beginning very early after hatching. *Proc. Natl. Acad. Sci. U.S.A.* **119**, e2122052119 (2022).
16. S. L. Tamm, Cilia and the life of ctenophores. *Invertebr. Biol.* **133**, 1–46 (2014).
17. C. Chun, *Die Ctenophoren Des Golfes von Neapel Und Der Angrenzenden Meeres-Abschnitte* (W. Engelmann, 1880).
18. P. Burkhardt, J. Colgren, A. Medhus, L. Digel, B. Naumann, J. J. Soto-Angel, E.-L. Nordmann, M. Y. Sachkova, M. Kittelmann, Syncytial nerve net in a ctenophore adds insights on the evolution of nervous systems. *Science* **380**, 293–297 (2023).
19. R. Hertwig, *Über Den Bau Der Ctenophoren - Studien Zur Blättertheorie* (G. Fischer, 1880).
20. M.-L. Hernandez-Nicaise, "Ctenophora," in *Biology of the Integument*, J. Bereiter-Hahn, A. G. Matoltsy, K. S. Richards, Eds. (Springer, 1984), pp. 96–111.
21. G. A. Horridge, Presumed photoreceptive cilia in a ctenophore. *J. Cell Sci.* **S3-105**, 311–317 (1964).
22. S. L. Tamm, "Ctenophora", in *Electrical Conduction and Behavior in "Simple" Invertebrates* (Shelton G. A. B., 1982), pp. 266–358.
23. C. Nielsen, Larval and adult brains. *Evol. Dev.* **7**, 483–489 (2005).
24. H. Marlow, M. A. Tosches, R. Tomer, P. R. Steinmetz, A. Lauri, T. Larsson, D. Arendt, Larval body patterning and apical organs are conserved in animal evolution. *BMC Biol.* **12**, 7 (2014).
25. E. Gilbert, J. Craggs, V. Modepalli, Gene regulatory network that shaped the evolution of larval apical organ in Cnidaria. *Mol. Biol. Evol.* **41**, msad285 (2024).
26. K. Z. Sabin, S. Chen, E. M. Hill, K. J. Weaver, J. Yonke, M. Kirkman, W. B. Redwine, A. M. L. Klompen, X. Zhao, F. Guo, M. C. McKinney, J. L. Dewey, M. C. Gibson, Graded FGF activity patterns distinct cell types within the apical sensory organ of the sea anemone Nematostella vectensis. *Dev. Biol.* **510**, 50–65 (2024).
27. W. A. Müller, T. Leitz, Metamorphosis in the Cnidaria. *Can. J. Zool.* **80**, 1755–1771 (2002).
28. H. Zang, N. Nakanishi, Expression analysis of cnidarian-specific neuropeptides in a sea anemone unveils an apical-organ-associated nerve net that disintegrates at metamorphosis. *Front. Endocrinol.* **11**, 63 (2020).
29. I. L. Dittmann, A. L. Grosbusch, M. Nagler, W. Salvenmoser, A. Zankel, M. J. Telford, B. Egger, The ultrastructure of the apical organ of the Müller's larva of the tiger flatworm *Prostheceraeus crozieri*. *Cell Biol. Int.* **47**, 1354–1367 (2023).
30. L. Piovani, D. J. Leite, L. A. Yañez Guerra, F. Simpson, J. M. Musser, I. Salvador-Martínez, F. Marlétaz, G. Jékely, M. J. Telford, Single-cell atlases of two lophotrochozoan larvae highlight their complex evolutionary histories. *Sci. Adv.* **9**, eadg6034 (2023).
31. M. Conzelmann, E. A. Williams, S. Tunaru, N. Randel, R. Shahidi, A. Asadulina, J. Berger, S. Offermanns, G. Jékely, Conserved MIP receptor–ligand pair regulates *Platynereis* larval settlement. *Proc. Natl. Acad. Sci. U.S.A.* **110**, 8224–8229 (2013).
32. C. Sinigaglia, H. Busengdal, L. Leclère, U. Technau, F. Rentzsch, The bilaterian head patterning gene *six3/6* controls aboral domain development in a cnidarian. *PLoS Biol.* **11**, e1001488 (2013).
33. E. Gilbert, C. Teeling, T. Lebedeva, S. Pedersen, N. Chrismas, G. Genikhovich, V. Modepalli, Molecular and cellular architecture of the larval sensory organ in the cnidarian *Nematostella vectensis*. *Development* **149**, dev200833 (2022).
34. L. Leclère, M. Bause, C. Sinigaglia, J. Steger, F. Rentzsch, Development of the aboral domain in *Nematostella* requires β-*catenin* and the opposing activities of *six3/6* and *frizzled5/8*. *Development* **143**, 1766–1777 (2016).
35. K. Pang, J. F. Ryan, N. I. S. C. Comparative Sequencing Program, J. C. Mullikin, A. D. Baxevanis, M. Q. Martindale, Genomic insights into Wnt signaling in an early diverging metazoan, the ctenophore *Mnemiopsis leidyi*. *EvoDevo* **1**, 10 (2010).
36. J. F. Ryan, K. Pang, N. I. S. C. Comparative Sequencing Program, J. C. Mullikin, M. Q. Martindale, A. D. Baxevanis, The homeodomain complement of the ctenophore *Mnemiopsis leidyi* suggests that Ctenophora and Porifera diverged prior to the ParaHoxozoa. *EvoDevo* **1**, 9 (2010).
37. M.-L. Hernandez-Nicaise, "Système nerveux et intégration chez les Cténaires. Etude ultrastructurale et comportementale," thesis, Univ. Claude Bernard, Lyon, France (1974).
38. S. L. Tamm, S. Tamm, Novel bridge of axon-like processes of epithelial cells in the aboral sense organ of ctenophores. *J. Morphol.* **254**, 99–120 (2002).
39. G. A. Horridge, Relations between nerves and cilia in Ctenophores. *Am. Zool.* **5**, 357–375 (1965).
40. M. Z. Aronova, Electron microscopy observation on the aboral organ of Ctenophora. I. The gravity receptor. *Z. Mikrosk. Anat. Forsch.* **88**, 401–412 (1974).
41. R. T. Moreland, A.-D. Nguyen, J. F. Ryan, A. D. Baxevanis, The Mnemiopsis Genome Project Portal: Integrating new gene expression resources and improving data visualization. *Database* **2020**, baaa029 (2020).
42. A. H. Fischer, K. Pang, J. Q. Henry, M. Q. Martindale, A cleavage clock regulates features of lineage-specific differentiation in the development of a basal branching metazoan, the ctenophore *Mnemiopsis leidyi*. *EvoDevo* **5**, 4 (2014).
43. K. Jokura, S. Jasek, L. Niederhaus, P. Burkhardt, G. Jékely, Neural connectome of the ctenophore statocyst. *eLife* **14**, RP108420 (2025).
44. S. L. Tamm, Functional consequences of the asymmetric architecture of the ctenophore statocyst. *Biol. Bull.* **229**, 173–184 (2015).
45. M. Y. Sachkova, E. L. Nordmann, J. J. Soto-Àngel, Y. Meeda, B. Górski, B. Naumann, D. Dondorp, M. Chatzigeorgiou, M. Kittelmann, P. Burkhardt, Neuropeptide repertoire and 3D anatomy of the ctenophore nervous system. *Curr. Biol.* **31**, 5274–5285.e6 (2021).
46. S. L. Tamm, A. G. Moss, Unilateral ciliary reversal and motor responses during prey capture by the ctenophore *Pleurobrachia*. *J. Exp. Biol.* **114**, 443–461 (1985).
47. R. Feuda, I. S. Peter, Homologous gene regulatory networks control development of apical organs and brains in Bilateria. *Sci. Adv.* **8**, eabo2416 (2022).
48. H. Yuan, W. L. Hatleberg, B. M. Degnan, S. M. Degnan, Gene activation of metazoan Fox transcription factors at the onset of metamorphosis in the marine demosponge *Amphimedon queenslandica*. *Dev. Growth Differ.* **64**, 455–468 (2022).
49. M. C. Coyle, A. M. Tajima, F. Leon, S. P. Choksi, A. Yang, S. Espinoza, T. R. Hughes, J. F. Reiter, D. S. Booth, N. King, An RFX transcription factor regulates ciliogenesis in the closest living relatives of animals. *Curr. Biol.* **33**, 3747–3758.e9 (2023).
50. J. J. Soto-Angel, E.-L. Nordmann, D. Sturm, M. Sachkova, K. Pang, P. Burkhardt, "Stable Laboratory Culture System for the Ctenophore *Mnemiopsis leidyi*," in *Ctenophores*, vol. 2757 of *Methods in Molecular Biology*, L. L. Moroz, Ed. (Springer, 2024), pp. 123–145.
51. A. Jan, M. Candelas, J. J. Soto-Angel, "Métodos de cultivo de zooplancton gelatinoso", in *Zooplancton Gelatinoso* (El Colegio de la Frontera Sur, ed. 1, 2026).
52. J. Schindelin, I. Arganda-Carreras, E. Frise, V. Kaynig, M. Longair, T. Pietzsch, S. Preibisch, C. Rueden, S. Saalfeld, B. Schmid, J.-Y. Tinevez, D. J. White, V. Hartenstein, K. Eliceiri, P. Tomancak, A. Cardona, Fiji: An open-source platform for biological-image analysis. *Nat. Methods* **9**, 676–682 (2012).
53. A. Cardona, S. Saalfeld, J. Schindelin, I. Arganda-Carreras, S. Preibisch, M. Longair, P. Tomancak, V. Hartenstein, R. J. Douglas, TrakEM2 software for neural circuit reconstruction. *PLOS ONE* **7**, e38011 (2012).

54. B. Schmid, J. Schindelin, A. Cardona, M. Longair, M. Heisenberg, A high-level 3D visualization API for Java and ImageJ. *BMC Bioinformatics* **11**, 274 (2010).
55. D. G. Mitchell, A. Edgar, M. Q. Martindale, Improved histological fixation of gelatinous marine invertebrates. *Front. Zool.* **18**, 29 (2021).
56. H. M. T. Choi, M. Schwarzkopf, M. E. Fornace, A. Acharya, G. Artavanis, J. Stegmaier, A. Cunha, N. A. Pierce, Third-generation in situ hybridization chain reaction: Multiplexed, quantitative, sensitive, versatile, robust. *Development* **145**, dev165753 (2018).
57. A. M. Elagoz, R. Styfhals, S. Maccuro, L. Masin, L. Moons, E. Seuntjens, Optimization of whole mount RNA multiplexed in situ hybridization chain reaction with immunohistochemistry, clearing and imaging to visualize octopus embryonic neurogenesis. *Front. Physiol.* **13**, 882413 (2022).
58. R. Derelle, H. Philippe, J. K. Colbourne, Broccoli: Combining phylogenetic and network analyses for orthology assignment. *Mol. Biol. Evol.* **37**, 3389–3396 (2020).
59. R. C. Edgar, MUSCLE: Multiple sequence alignment with high accuracy and high throughput. *Nucleic Acids Res.* **32**, 1792–1797 (2004).
60. S. Capella-Gutiérrez, J. M. Silla-Martínez, T. Gabaldón, trimAl: A tool for automated alignment trimming in large-scale phylogenetic analyses. *Bioinformatics* **25**, 1972–1973 (2009).
61. B. Q. Minh, H. A. Schmidt, O. Chernomor, D. Schrempf, M. D. Woodhams, A. Von Haeseler, R. Lanfear, IQ-TREE 2: New models and efficient methods for phylogenetic inference in the genomic era. *Mol. Biol. Evol.* **37**, 1530–1534 (2020).

Acknowledgments: The ctenophore culture at Oxford Brookes was supported by an Oxford Brookes University Research Excellence Award. High-pressure freezing and SBFSEM and transmission electron microscopy (TEM) imaging were conducted in the Oxford Brookes Centre for Bioimaging. We thank R. Feuda for discussion on apical gene regulatory networks in animals, S. Richter and C. Wirkner for discussions on metazoan larvae, and Burkhardt Lab members for discussion and feedback on the study. **Funding:** This work was supported by the Michael Sars Centre core budget, the European Research Council (ERC Consolidator Grant 101044989 "ORIGINEURO" awarded to P.B., supporting A.F., J.C., and C.L.G.), and the Human Frontier Science Program (grant RGP025/2023 to P.B.). **Author contributions:** Conceptualization: A.F., B.N., J.C., M.K., and P.B. Methodology: A.F., J.C., C.L.G., J.J.S.-A., A.J., M.K., and P.B. Investigation: A.F., L.D., D.S., J.C., M.K., and P.B. Visualization: A.F., L.D., J.C., M.K. and P.B. Resources: J.J.S.-A., A.J., M.K., and P.B. Formal analysis: A.F., L.D., D.S, M.K. and P.B. Validation: A.F., M.K., and P.B. Data curation: A.F., L.D., and M.K. Writing—original draft: A.F. and P.B. Writing—review and editing: A.F., L.D., D.S., J.C., C.L.G., J.J.S.-A., A.J., B.N., M.K., and P.B. Supervision: P.B. Project administration: P.B. Funding acquisition: M.K. and P.B. **Competing interests:** The authors declare that they have no competing interests. **Data, code, and materials availability:** All data and code needed to evaluate and reproduce the results in the paper are present in the paper and/or the Supplementary Materials. HCR probes can be obtained from the corresponding authors upon request. Raw SBFSEM datasets can be found at https://doi.org/10.6084/m9.figshare.29314115.v1.

Submitted 22 July 2025
Accepted 6 February 2026
Published 4 March 2026
10.1126/sciadv.aea8399

ScienceAdvances

The 3D architecture of the ctenophore aboral organ and the evolution of complex integrative centers in animals

Anna Ferraioli, Leonid Digel, Daniela Sturm, Jeffrey Colgren, Carine Le Goff, Alexandre Jan, Joan J. Soto-Angel, Benjamin Naumann, Maike Kittelmann, and Pawel Burkhardt

Sci. Adv. **12** (10), eaea8399. DOI: 10.1126/sciadv.aea8399

Science Advances (ISSN 2375-2548) is published by the American Association for the Advancement of Science. 1200 New York Avenue NW, Washington, DC 20005. The title *Science Advances* is a registered trademark of AAAS.